Topology-Aware Fingerprint Representation Using Graph Convolutional Network for Robust Minutiae Refinements

Yoogesh A[1], Rama Prasath A[2]*
Research Scholar-Department of Computer Applications
SRM Institute of Science and Technology, Tiruchirappalli, India 621105[1]
Department of Computer Applications, SRM Institute of Science and Technology,
Tiruchirappalli, India 621105[2]

***Abstract*—Most of the fingerprint recognition systems represent minutiae as independent points. This reduces robustness under noise, distortion, and partial impressions. The lack of explicit structural modeling contributes to inconsistent feature reliability, specifically in defocused acquisition conditions. To address these limitations, a Topology-Aware Graph Convolutional Network (Topo-GCN) is proposed. Topo-GCN is a geometric fingerprint representation framework that treats all minutiae points as interrelated nodes and polishes them using a Graph Convolutional Network (GCN). Each node is represented as a 14-dimensional descriptor with the Multi-scale Spatial Feature Tensor (MSFT) technique. A novel Relational Connection Factor (RCF) applies adaptive topology-aware learning to construct edges in place of traditional distance-based graph construction. The Hybrid scoring technique combines learned node representations with graph-theoretic measures to separate genuine minutiae from false ridge information. Furthermore, a lightweight pseudo-labeling scheme efficiently trains the model without depending on the large-scale annotated datasets. The proposed Topo-GCN framework achieves an Area under Curve (AUC) of 0.9614, 0.9769, and 0.9831 with consistent verification performance (EER) of 1.85%, 1.39%, and 1.64% and stable relational encoding with mean edge weights of 0.712, 0.739, and 0.758 across FVC2000, FVC2002, and FVC2004 datasets. The results indicate that integrating relational topology into minutiae modeling considerably enhances robustness, making Topo-GCN a viable approach for secure and efficient fingerprint authentication systems.**

Keywords*—Biometric authentication; fingerprint recognition; Graph Convolutional Network; minutiae refinement; topology-aware representation

I. Introduction

The modern technological era demands high-security systems with a relatively low computational complexity for individual authentication. The inherent vulnerability of password- and token-based authentication mechanisms to security breaches highlights the necessity for developing more robust and reliable alternatives. In this regard, biometric authentication relies on characteristics that are intrinsically associated with an individual, whereas former methods depend on knowledge that can be guessed and imitated.

The computationally inexpensive algorithm requirement narrows down to the utilization of unimodal biometric techniques rather than a multimodal approach that requires heavy processing. Among various traits, fingerprints are superior due to their uniqueness and permanence. Additionally, fingerprint sensors are cost and space-efficient compared to other biometric sensors, as they can be integrated to authentication device with a minimal modification. Similar to traditional techniques, fingerprint-based authentication systems are vulnerable to attacks. Following a successful security breach, unlike password reset, fingerprints cannot be replaced. Therefore, protecting stored fingerprint template against inversion, linkage, and replay attacks is important. Cancelable template approach satisfies the properties of diversity, irreversibility, revocability and unlinkability. Minutiae extraction is one of the keystages in the fingerprint authentication system pipeline.

Existing minutiae extraction approaches rely on handcrafted rules, which often fail to capture the relational structure among minutiae points [1]. They are sensitive to noise and lacks generalization, and may discard valid minutiae. Furthermore, these schemes do not explicitly exploit topological dependencies [2]. The importance of relational and spatial dependency modeling has also been shown in graph-based spatial processing frameworks [3]. These limitations motivate the need for a structurally aware and learnable refinement mechanism.

The major contributions of this work are summarized as follows:

- A hybrid fingerprint processing framework that combines MSFT-driven texture encoding with a learnable graph-based refinement, allowing structurally aware minutiae validation without high computational complexity.
- A novel graph-oriented clipping technique replaces conventional rule-based filtering with adaptive node scoring derived from the feature quality, connectivity pattern, and relational consistency measures.
- Achieving better storage efficiency and improved matching performance by generating a compact and unique representation with selective node retention and the graph embedding technique.

II. Related Work

Techniques related to fingerprint minutiae extraction have advanced considerably. Existing fingerprint recognition sys-

*Corresponding author

tems rely on either one of the following techniques described below. Each technique has a unique way of feature representation. Traditional minutiae extraction approaches primarily rely on Crossing Number (CN) and Gabor filtering, which extract Standard Minutiae Triplets (SMT). These methods suffer from sensor noise, scaling and translation. Recent deep learning-based methods attempt to learn feature representations directly from data, introducing heatmap-based and descriptor-based representations, but ignores intrinsic topological relationships among minutiae. Global representation models rely on fixed-length embeddings rather than conventional technique. Such models are computationally efficient with reduced discriminative capability. Hybrid approaches combine local and global minutiae information to create a balanced structural and statistical representations. However, they still depend on heuristic design choices and does not support adaptive relational modeling. SDK-dependent systems rely on proprietary black-box extractors such as VeriFinger and MegaMatcher. They are limited to reproducibility and end-to-end optimization. The comparative analysis of these approaches is summarized and given below.

The classical minutiae extraction methods include a Gabor filter-based linear band-pass approach utilized to compute local ridge frequency and orientation [1], where Standard Minutiae Triplets (SMT), i.e., spatial coordinates (x, y) and the orientation angle (theta) for ridge endings and bifurcations, are extracted; however, reliance on a centroid-based reference point for coordinate translation is mathematically unstable because the addition of a single false minutia alters the entire coordinate system [1]. The Crossing Number (CN) approach [2] is also utilized, but the Crossing Number (CN) algorithm is incapable of distinguishing between legitimate biological traits and topological artifacts [2].

Similarly, a Gabor filter-based extraction approach [4] depends on a singular global reference point (core point) for the Mobius transformation, which is sensitive to registration jitter, where a one-pixel shift in the reference point causes a total non-linear divergence of the transformed coordinates [4]. The Adaptive Scale-Invariant Feature Transform (SIFT) detector [5] extracts 128-dimensional feature vectors consisting of SMT derived from local gradient histograms; however, SIFT is mathematically designed to locate extrema in continuous intensity gradients, which are destroyed by the binarization and thinning process [5]. The Fingerprint Manual Minutiae Marker (FM3) toolkit [6] utilizes the ISO/IEC 19794-2 triplet, but the use of manual extraction introduces a human subjective error [6].

These paradigms treat minutiae as isolated features, explicitly lacking in learning and modeling the relational topology.

Deep learning-based minutiae extraction methods include a CSPNet-based extractor (adapted Cross Stage Partial Network) trained via knowledge distillation from FingerNet [7], extracting SMT and a confidence level for each minutia; however, the feature extractor limits system performance and mimics the systematic errors and biases due to the reliance on FingerNet knowledge [7]. DeepPrint, a multi-branch deep network that incorporates a minutiae-map detection branch to guide representation learning [8], encodes SMT as a 6-channel heatmap, but discards the local relative topological distances between minutiae, making the system vulnerable to false accepts in high inter-class similarity [8]. A ResNet50-Transformer Minutiae Map Predictor [9], which utilizes a ResNet50 backbone coupled with self-attention transformer layers to predict a 12-channel heat map, extracts SMT and a 96-dimensional descriptor for each minutia patch; however, the reliance on fixed 96×96 patches alters the local texture relative to the minutiae center [9]. Deep learning-based methods improve feature representations by operating on the pixel-level suggestions and failing to encode inter-minutiae relationships.

Global representation models include fixed-length representations [10], where textural cues and minutiae representations are concatenated into a 512-dimensional fixed-length feature vector, but the relative geometric distances between minutiae are ignored [10]. A customized SVM classification model (C-SVM-Cl) [11] maps global P-Hash vectors directly to a biometric identifier (BID), using a 64-bit global hash vector derived from the frequency domain of the fingerprint image, but abandoning local minutiae sacrifices high-entropy discriminative features, resulting in a mediocre 75% accuracy [11]. ShuffleNetv2.3-based architectures [12] extract high-level hierarchical feature vectors as global embeddings; however, the system is spatially variant, lacking rotation and translation invariance and will fail if the input image is not perfectly aligned [12]. Fully minutiae-free approaches utilizing a DINOv2-Base Vision Transformer backbone [13] produce a 1536-dimensional global embedding from the [CLS] token of the final Transformer layer, but lack explicit topological invariance, making the recognition performance highly volatile [13]. Dilated Convolutional Neural Network (DICNN) [14] extracts local and global structural properties such as singularities and ridgeline shapes, but a gridding effect causes sparse spatial sampling that ignores contiguous ridge-valley connectivity [14]. Hierarchical Heterogeneous Ant Colony Optimization based Fingerprint Matching (HHACOFM) [15] relies on ridge topology matching using a boolean matrix representation, but depends entirely on ant agents to compensate for translational and rotational shifts [15]. Pre-trained VGG16 and VGG19 backbones [16] extract high-dimensional global latent embeddings, but lack rotation and translation invariance [16]. A ViT-based Siamese Network [17] produces 256-dimensional representations, but the ResNet-18 front-end discards high-frequency ridge-valley details necessary for sub-pixel localization accuracy [17]. Attention-based and CNN-based classification heads [18] extract global embeddings and local feature maps, but reliance on an external spatial alignment module leads to catastrophic misalignment if inaccurate [18]. Log Gabor feature vectors [19] generate a 477,144-dimensional feature space, but introduce redundancy and increase false positives [19]. CNN-based descriptors utilizing AlexNet [20] produce fixed-size latent feature vectors, but the architecture is incapable of resolving fine-grained ridge-line singularities [20].

The fixed-length global embeddings suppress local geometric relationships. These abstractions discard the reliable discriminative structural information.

Hybrid representations include ResNet50 with multihead attention for global feature extraction [21], extracting SMT, but Sobel-based enhancement cannot distinguish between legitimate ridge boundaries and high-frequency noise artifacts [21]. Minutiae triplet-based feature extraction [22] produces a

6D feature vector including spatial distance, ridge count, and ridge density, but handcrafted topology is sensitive to non-linear skin deformation [22].

Hybrid techniques combine local and global information but still rely on predefined handcrafted features and lacks adaptive modeling.

SDK-dependent systems include COTS SDK (MegaMatcher) [23], extracting SMT of angular sectors, but exhibiting a rotation offset that breaks feature interoperability [23]. VeriFinger SDK 12.0 [24] utilizes paired control points for Thin Plate Spline (TPS) transformation, but errors in the initial transformation cannot be corrected [24]. VeriFinger SDK [25] extracts SMT and core points but is incapable of anchoring focal points in arch patterns [25]. VeriFinger SDK 12.1 [26] used for ground truth extraction prevents gradient-based backpropagation of minutiae-specific loss [26]. Rule-based SDK extraction [27] fails in low-quality regions. VeriFinger 11.1 SDK [28] introduces an opaque dependency preventing optimization. MindTCT with VeriFinger 12.1 [29] constrains the system to classical ridge-following rules. VeriFinger 4.0 SDK [30] fails to distinguish biological singularities from sensor noise. VeriFinger v12.0 [31] introduces circular dependency in degraded regions. Multi-extractor frameworks [32] relying on commercial SDKs create gradient disconnection, preventing optimization of identity loss.

SDK-dependent minutiae extraction methodologies prevent end-to-end optimization and limits the integration of learnable structural representations.

Most state-of-the-art approaches struggle to remain stable with noisy, distorted, and incomplete fingerprint impressions. These limitations necessitate a framework that can capture and adaptively fine-tune the inter-minutiae associations. Topo-GCN models the fingerprint data as a graph, where minutiae are represented as nodes and the structural interactions are encoded through edges, enabling effective learning of relational dependencies.

III. Proposed Work

Despite wide range of advancements, fingerprint-based identification systems validate each minutia independently from the local topology surrounding it. However, ridges are continuous flow fields driven by parallel direction and frequency of directions. Evaluating the isolated minutiae alone creates a structural ambiguity such that spurious detections from noise and broken ridges cannot be categorically separated from real minutiae. Utilizing isolated minutiae to determine the validity of the feature struggles with partial impressions, sensor noise, and elastic distortion. To alleviate this issue, existing methods rely on the enhancement of local descriptors or the learning of global structure of fingerprints. Local descriptors cannot enforce consistency among structures that are spatially distributed, while global embedding models succeed in creating fixed-length representations of fingerprints, downgrading the direct geometric relationship between minutiae. Therefore, both methods provide feature space representations that do not explicitly encode the topological relationship between features, creating instability under occlusion, deformation, and acquisition noise.

A prerequisite to implement meaningful representation of minutiae is to have the ability to establish consistency of relationships amongst minutiae. Therefore, the validity of any given minutia can be determined jointly with neighboring ridge structures. This can be accomplished by retaining both the local features and the underlying topological structure of the fingerprint. Modeling fingerprint minutiae using a graph offers the ideal framework for encoding inter-relational minutiae relationships. However, conventional, naïve graph representations are solely based on spatial proximity and do not reflect the physical continuity of ridge flow, resulting in connectivity problems.

To address these limitations, Topo-GCN framework will define a relational representation that is constrained by ridge-level physical properties and polishes through learnable inference. The proposed approach differs from the traditional approaches by modeling minutiae as a graph and treating it as the primary mechanism of representation. Thus, the validity of a specific minutia arises from structural agreement and not from feature confidence.

In this formulation, the Graph Convolutional Network (GCN) serves an additional purpose beyond merely aggregating features but enforcing consistency across the entire graph. The network iteratively propagates through all of its neighbouring nodes and eliminates the nodes that exhibit structural inconsistency. The utilization of the GCN in the Topo-GCN framework serves as a means of providing distributed relational reasoning via global embedding strategies. The proposed framework shifts minutiae extraction from a detection problem to a consistency-driven inference problem over a structured topological domain.

Fig. 1 illustrates the architecture of the proposed Topo-GCN framework. The extracted fingerprint feature set is represented as a structured graph. Each node encodes a candidate minutia characterized by descriptors derived from the Multi-scale Spatial Feature Tensor (MSFT), including spatial position, orientation with texture, structural, and multi-scale information.

Edges are constructed using the range-restricted connectivity scheme by capturing local ridge topology. The resultant graph is processed with the learnable GCN to adaptively filter node representations by discarding structurally inconsistent candidates. The refinement process improves distinctness by utilizing the learned feature interactions and eliminates the requirement for large-scale training.

A composite scoring mechanism evaluates each node based on a weighted combination of feature confidence, degree centrality, and edge consistency. The nodes with the score exceeding an adaptive threshold are retained, whereas the nodes with low scores are ignored to preserve genuine structural patterns

The proposed scheme inherently supports robustness, compactness, and resistance to direct inversion as the final representation contains relational and topological dependencies rather than raw biometric features.

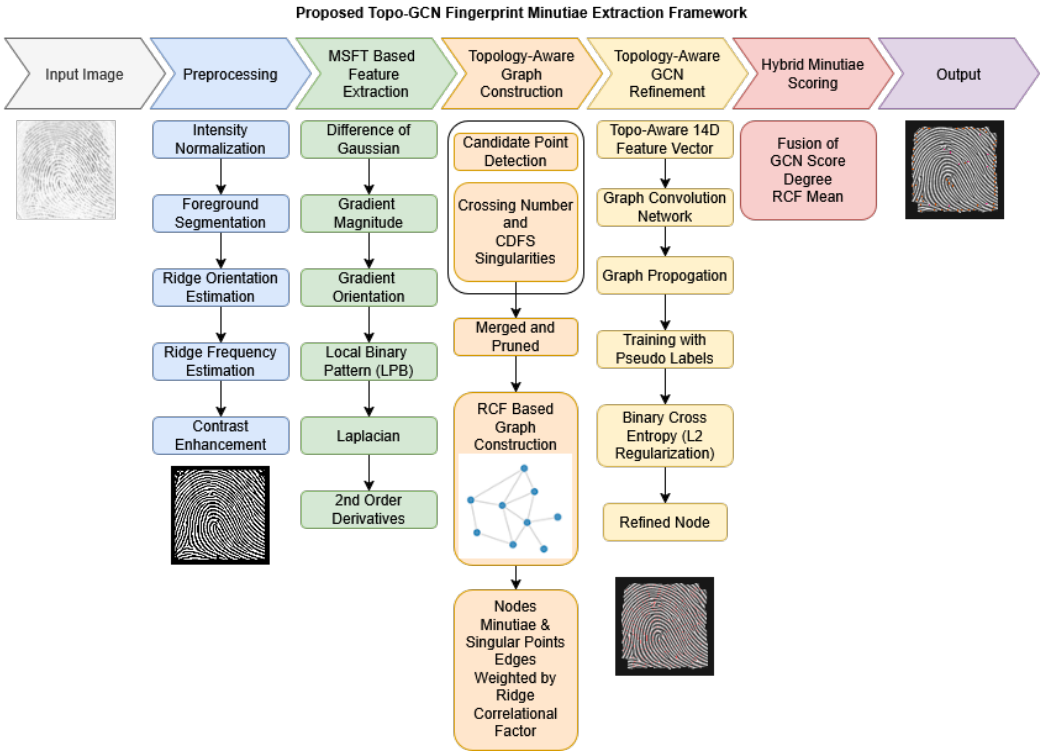

Fig. 1. Proposed fingerprint minutiae extraction framework.

A. Minutiae Representation

The minutiae representation is a three-layered hierarchical construct rather than a single vector. Each detected minutia is represented by a 14-dimensional feature vector X_i used for GCN inference. The feature vector comprises normalized spatial coordinates and orientation (θ/π), local coherence, minutiae type, and mean Ridge Connection Factor (RCF) with seven channels of MSFT to capture ridge-valley contrast. Furthermore, the degree of the node within the RCF graph encodes local structural connectivity. This formulation overcomes the conventional descriptor by redefining minutiae as a relational property instead of an isolated measurement.

The 14-dimensional descriptor represents the minutiae along with the local structural context. This is sufficient for subsequent graph learning.

Unlike DeepPrint, which treats minutiae as parts of a global image map, the proposed system builds a Relational Connection Factor (RCF) graph to capture innate relationships among minutiae. The edge weights f_r are defined as the fusion of Correlation Coefficient r_{cc}, Orientation Consistency o_c, and Frequency Consistency f_c, enabling a physical relationship between minutiae. Ridge flow interruption due to poor sensor contact causes the RCF weight to drop, enabling the GCN to de-weight the error node for better minutiae refinement. The RCF serves as a proxy for ridge-flow continuity. The model extracts structurally consistent minutiae from ridge irregularities, as in Eq. (1):

$$f_r(i,j) = \alpha \cdot r_{cc}(i,j) + \beta \cdot o_c(i,j) + \gamma \cdot f_c(i,j) + \delta \cdot e^{-d_{ij}/\sigma} \quad (1)$$

B. Alignment-Free Property

DeepPrint relies on an "Alignment Module" to orient the fingerprint before feature extraction. Topo-GCN logic is alignment-free and learns the relative topology between nodes. The graph structure remains identical whether the fingerprint is rotated or shifted, provided the relative distances between minutiae are preserved.

The reliance on reference point estimation is eliminated, and the invariance is enforced through relational geometry to make the representation inherently robust to positional variations without explicit normalization.

C. Graph Construction

Instead of Euclidean distance to define graph edges, Topological Relational Construction (TRC) is a parametrically adaptive graph structure that fuses domain-driven constraints with learnable refinement.

The nodes are a fusion of Crossing Number (CN) minutiae and CDFS singularity candidates. Unlike standard pipelines that accept all detected points, the proposed technique prunes them using a coherence threshold and a foreground mask. The pruning criterion is adaptively modulated during training so that the model retains the low-confident yet structurally informative points.

Edge formation is constrained within a local neighborhood. The connectivity is modeled as a continuous function of Euclidean distance D with soft distance-dependent weighting to enable adaptive neighborhood formation.

Each edge is defined through a learnable fusion of structural cues. The edge weight is formulated, as in Eq. (2):

$$f_r(i,j) = W^T \cdot \phi(i,j) \tag{2}$$

where,

$$\phi(i,j) = [r_{cc},\ o_c,\ f_c,\ e^{-d_{ij}/\sigma}]$$

and W is the learnable parameter vector. Initially, the graph is constructed with fixed ridge-based rules and subsequently refined during training through learnable weighting.

D. GCN Adjacency Matrix

For graph convolution, the adjacency matrix is constructed using the refined edge weights and normalized, as in Eq. (3):

$$\hat{A} = D^{-\frac{1}{2}}(A + I)D^{-\frac{1}{2}} \tag{3}$$

This normalization ensures to distribute relational influence across structurally consistent neighborhoods. Furthermore, the dominance of spurious connections are prevented and true topological interactions are preserved.

E. GCN Propagation

The model propagates through a $14 \rightarrow 32 \rightarrow 16 \rightarrow 1$ architecture in Eq. (4), Eq. (5), and Eq. (6):

$$H_1 = \sigma(\hat{A}X_{\text{norm}}W_1) \tag{4}$$

$$H_2 = \sigma(\hat{A}H_1W_2) \tag{5}$$

$$s_c = \text{Sigmoid}(\hat{A}H_2W_3) \tag{6}$$

The propagation does not end with the GCN output. The final score is obtained, as in Eq. (7):

$$s_{\text{final}} = w^T[s_c,\ d_{\text{norm}},\ \text{RCF}_m] \tag{7}$$

which is the learnable fusion of GCN inference, node centrality, and ridge continuity, enabling adaptive weighting of structural cues.

GCN functions as a mechanism for propagating each node iteratively to validate it against its spatial neighborhood.

F. Global Descriptor Construction

Following graph-based learning, a higher-level 80-dimensional global descriptor is constructed for verification and validation, as in Eq. (8):

$$F = [H^{32}_{\text{ori}},\ H^{8}_{\text{freq}},\ S^{8}_{\text{min}},\ C^{16}_{\text{cyl}},\ S^{8}_{\text{graph}},\ S^{8}_{\text{ridge}}] \in \mathbb{R}^{80} \tag{8}$$

H^{32}_{ori} and H^{8}_{freq} denote the 32-bin orientation and 8-bin ridge frequency, respectively. These capture the overall directional and periodic characteristics of the fingerprint. The first- and second-order statistics of spatial coordinates, orientation, and local coherence are summarized in S^{8}_{min}.

C^{16}_{cyl} captures the local neighborhood structure by evaluating the average orientation distribution within local patches centered at each minutiae. S^{8}_{graph} handles relational consistency by aggregating GCN-derived node quality score, density, and node degree statistics. S^{8}_{ridge} determines ridge-level quality and consistency by incorporating contrast and image quality metrics.

The proposed descriptor sustains connectivity by ensuring that global representation retains the topology of the fingerprint instead of abstracting it and maintaining a compact representation for efficient storage and better processing [33].

G. Learning Strategy

The Topo-GCN framework integrates domain-driven constraints with learnable optimization, thereby avoiding reliance on fixed heuristic formulations. The edge weighting function $f_r(i,j)$ is defined as a fusion of correlation, orientation, frequency consistency, and distance decay, capturing the structural relationships between minutiae. The contribution weights $\alpha, \beta, \gamma, \delta$ govern this combination during graph construction. Although not explicitly learned, their effect is reflected in the learned transformations of node features and adjacency normalization within the GCN refinement stage, eliminating the need for manual tuning.

Furthermore, the structural cues are optimized indirectly with respect to the binary cross-entropy objective through the learning dynamics of the network.

A pseudo-labeling strategy is adopted to enable effective learning without depending on manually labelled datasets. The strategy programmatically classifies candidate minutiae based on structural integrity and connectivity measures. High-coherence and well-connected nodes are treated as positive samples, and low-confidence candidates are treated as negative samples. This facilitates a lightweight supervised training paradigm using mini-batch optimization with binary cross-entropy loss and regularization. To overcome the collapse of label distributions, class imbalance, and enhanced meaningful supervision, percentile-based fall back strategies are applied.

IV. Results and Discussion

Experimental analysis of the proposed Topo-GCN shows that learning over a 14-dimensional feature representation (X) provides better discriminative capability and generalization

performance compared to raw pixel-based modeling by achieving a training accuracy of 99.80% relative to 97.50%, as reflected in verification metrics.

The necessity for collaborative feature learning increases the complexity of raw image-based models during registration and matching the fingerprint. The proposed framework introduces a closely aligned representation directly encoding ridge coherence and alignment position. This shift enables targeted graph-based refinement, reducing the reliance on deep convolutional architectures.

The Topo-GCN framework segregates structural feature encoding from relational refinement by decoupling representational redundancy. This allows the model to emphasize on learning meaningful inter-minutiae dependencies through graph-based processing.

The architectural design ($14 \rightarrow 32 \rightarrow 16 \rightarrow 1$) enables better optimization within a reduced, information-bound space. This is substantiated with a mean processing time of 0.543 seconds and throughput of 1.84 images per second.

The reduced computational complication is due to the structured feature processing, unlike repeated high-dimensional convolutions.

The stable structural encoding and robustness of the representation are supported by the ridge-flow stability metrics, accomplishing a low orientation field error of 0.0126 rad and high coherence with a mean of 0.913. The topology-aware sparse graph with low graph density (0.0215–0.0312) and controlled mean node degree (2.34–3.27) limits unnecessary connectivity between nodes and the potential for over-smoothing via graph convolution. Therefore, node representations remain discriminative by preserving local ridge relationships and leading to improved separation between genuine and impostor score distributions.

Furthermore, the mean RCF edge weight (≈ 0.797) with low variance indicates stable relational encoding across varying fingerprint qualities. This suggests that the edge construction process is not significantly influenced by noise-sensitive features.

Stable relational modeling reinforces edge weighting (mean = 0.797) to maintain local feature interactions to remain discriminative.

Integrating local cylinder descriptors with global 80-dimensional feature embeddings by the hybrid scoring framework strengthens the verification reliability.

Effective separation between genuine (mean ≈ 0.80) and impostor (mean ≈ 0.25) distributions is achieved with the application of $\tanh$-based normalization, which induces a non-linear redistribution of similarity scores.

The overlap in the decision space and enhanced discriminability are attained with the margin amplification. Jointly, these results indicate that the proposed framework achieves enhanced verification performance through a synchronized blueprint that consolidates graph-structured learning and distribution-aware score normalization.

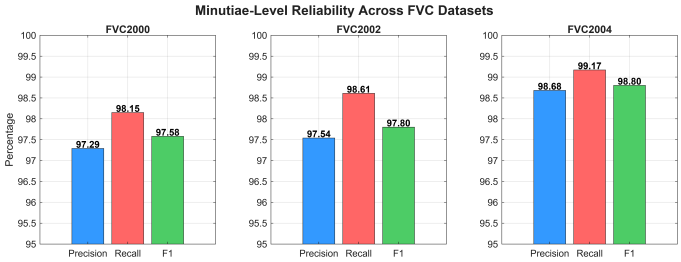

Fig. 2. Visual representation of precision, recall, and F1 score across FVC datasets.

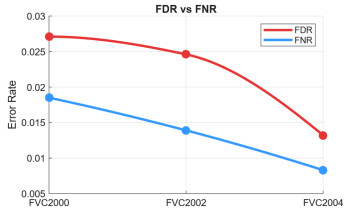

Fig. 3. False Discovery Rate vs. False Negative Rate.

A. Minutiae-Level Reliability (MLR)

To assess the ability of the Topo-GCN framework to filter appropriate candidates, precision, recall, and F1-score are determined. To ensure the successful elimination of noise and retention of genuine ridge features, False Discovery Rate (FDR) and False Negative Rate (FNR) are drawn.

Table I signifies strong minutiae-level reliability across all FVC datasets with F1-scores recorded at 97.58%, 97.80%, and 98.80%, respectively.

As shown in Fig. 2, precision, recall, and F1-score are higher and consistent compared to the state-of-the-art approaches. The higher values of recall suggest greater retention of true minutiae, despite the acquisition conditions.

Moreover, the precision value denotes that the graph-based refinement technique protects true ridge patterns and serves as a strong baseline compared to [14].

Based on the data in Table II, both False Detection Rate (FDR) and False Negative Rate (FNR) decreases from 0.0132 to 0.0083 across datasets denotes the stability of the refinement process.

The proposed framework maintains a strong balance by reducing false detections and preserving true minutiae. The proposed model adjusts to varying quality datasets and does not overfit.

Fig. 3 shows stable refinement behavior. Furthermore, the structural graph-based refinement filters the candidates based on relational consistency rather than isolated feature confidence is one among the improvements over the numerical baseline methods based on trade-off between FDR and FNR.

Table III indicates that the range growing from 2.50 to 3.01, the statistical distance between genuine and impostor score distributions.

Table IV shows that the proposed method achieves lower

TABLE I. MINUTIAE-LEVEL RELIABILITY ACROSS FVC DATASETS

Method	FVC2000			FVC2002			FVC2004		
	Prec.	Rec.	F1	Prec.	Rec.	F1	Prec.	Rec.	F1
[2]	97.13	96.84	96.99	96.29	95.74	96.01	96.5	95.8	96.1
[7]	86.76	89.58	88.51	90.76	91.42	91.09	84.8	86.6	85.7
[14]	96.50	97.69	97.09	95.81	94.96	95.38	98.63	98.47	98.55
[16]	94.42	91.36	92.86	93.64	92.88	93.26	92.6	92.4	92.4
Proposed	97.29	98.15	97.58	97.54	98.61	97.80	98.68	99.17	98.80

TABLE II. FALSE DETECTION RATE (FDR) AND FALSE NON-MATCH RATE (FNR) ACROSS DATASETS.

Dataset	FDR	FNR
FVC2000	0.0271	0.0185
FVC2002	0.0246	0.0139
FVC2004	0.0132	0.0083

TABLE III. SEPARABILITY INDEX (d')

Metric	FVC2000	FVC2002	FVC2004
d' separability	2.50	2.83	3.01

EER across all datasets, outperforming existing methods, particularly on FVC2002 with 1.39%.

Table V further confirms the discriminative capability, achieving AUC values of 0.9614, 0.9769, and 0.9831 for the FVC datasets, respectively.

Fig. 4 shows strong ROC performance, with consistent curves across datasets.

A consistent improvement with the shift in score distributions is observed. The genuine scores cluster around 0.80 while impostor scores remain near 0.25. The hybrid scoring mechanism reinforces the separation by fusing GCN outputs with node degree and ridge continuity. The tanh-based normalization minimizes overlap in the decision space by amplifying decision margins through a non-linear redistribution of similarity scores.

The preprocessing stage influences the graph modeling. Table VI populated with high PSNR and SSIM, significant improvement in CNR, and lower MSE and OFE. This illustrates the necessity of conserving structural information of the image prior to feature extraction [34].

Fig. 5 graphically illustrates the preprocessing and minutiae extraction pipeline. Fig. 6, indicate that the proposed Topo-GCN has improved the quality of the image with stable ridge flow.

Table VII showcases that the low graph density (0.0215–0.0312) and controlled node degree (2.34–3.27) prevent over-smoothing during graph convolution. The existence of clear separation between the GCN score distributions of genuine versus imposter supports the hypothesis that the learned representations of nodes accurately reflect the unique topology of the associated minutiae as opposed to only using local feature descriptors. Therefore, explicit relational modelling improves fingerprint discriminability.

To evaluate RCF edge-weight formulation as in Eq. (1), each component was removed independently to understand the contribution of each term. Table VIII presents the results of the evaluation. Removal of any one of the terms lead to a sharp increase in the EER. The exclusion of r_{cc} recorded the highest EER. The complete formulation of RCF achieved the minimal EER.

TABLE IV. COMPARISON OF EQUAL ERROR RATE (EER)

Models	FVC2000	FVC2002	FVC2004
[5]	2.96	2.36	2.01
[6]	1.38	2.47	1.85
[13]	2.02	2.18	3.48
[17]	2.07	1.61	1.73
[21]	1.85	1.95	2.20
Proposed	1.05	1.39	1.64

TABLE V. AREA UNDER THE CURVE (AUC) ACROSS FVC DATASETS

FVC2000	FVC2002	FVC2004
0.9614	0.9769	0.9831

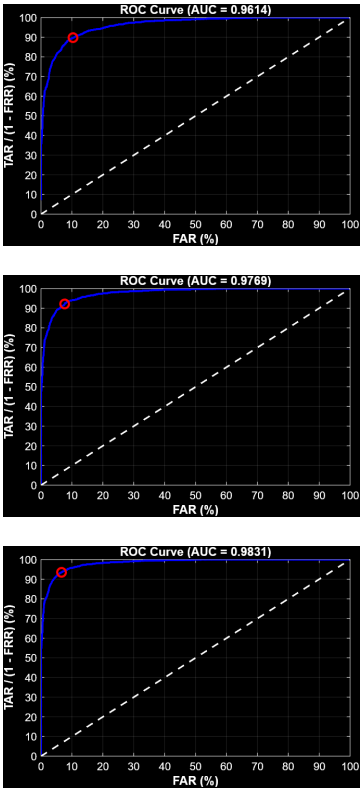

Fig. 4. Receiver Operating Characteristic (ROC) curves of the proposed Topology-Aware Graph Convolutional Network (Topo-GCN): (**a**) FVC2000; (**b**) FVC2002; (**c**) FVC2004.

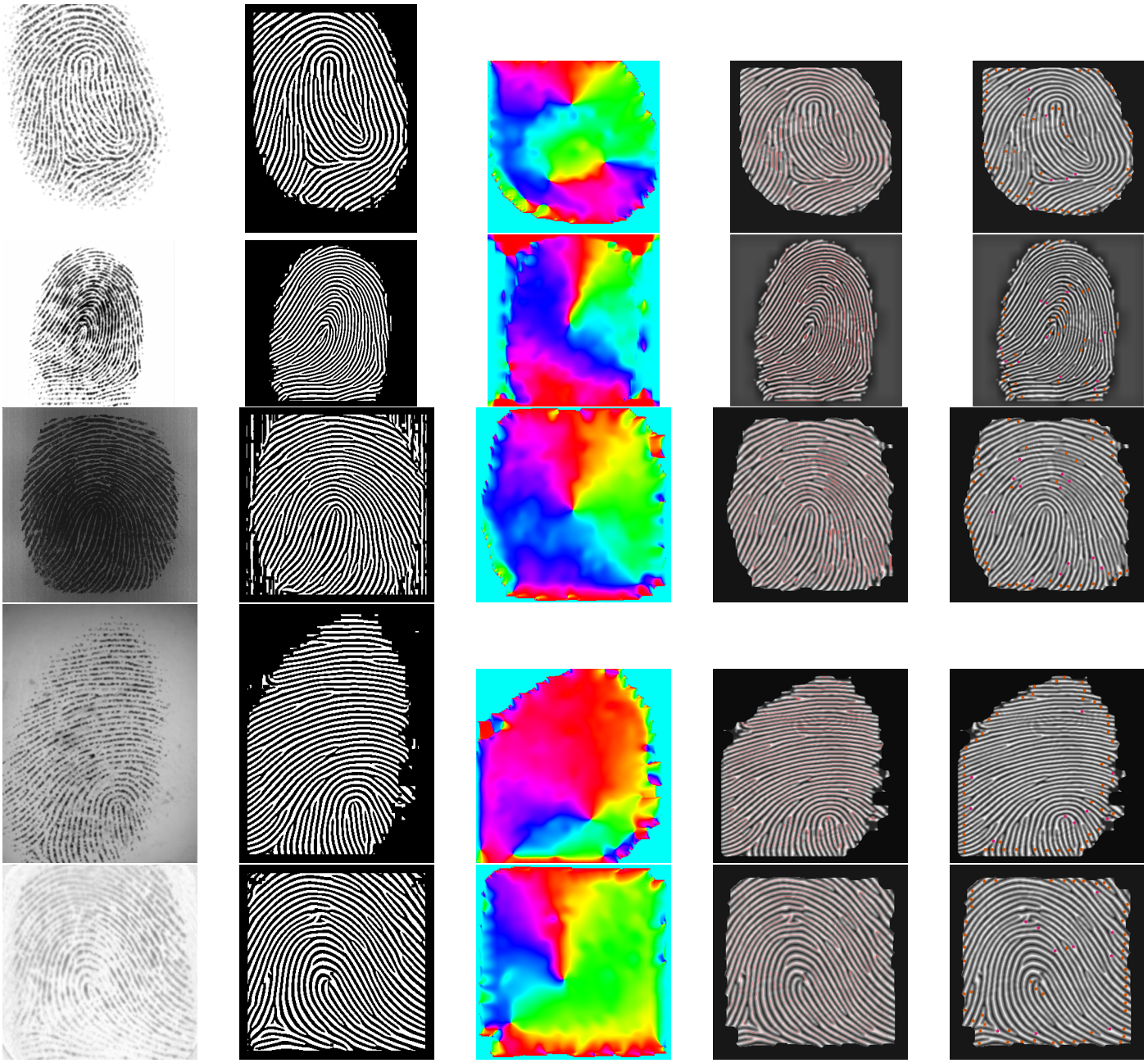

Fig. 5. Qualitative visualization of fingerprint preprocessing and minutiae extraction. Each row corresponds to a different fingerprint sample. Columns (left to right) represent: input image, enhanced image, orientation field estimation, skeletonized ridge structure, and extracted minutiae points.

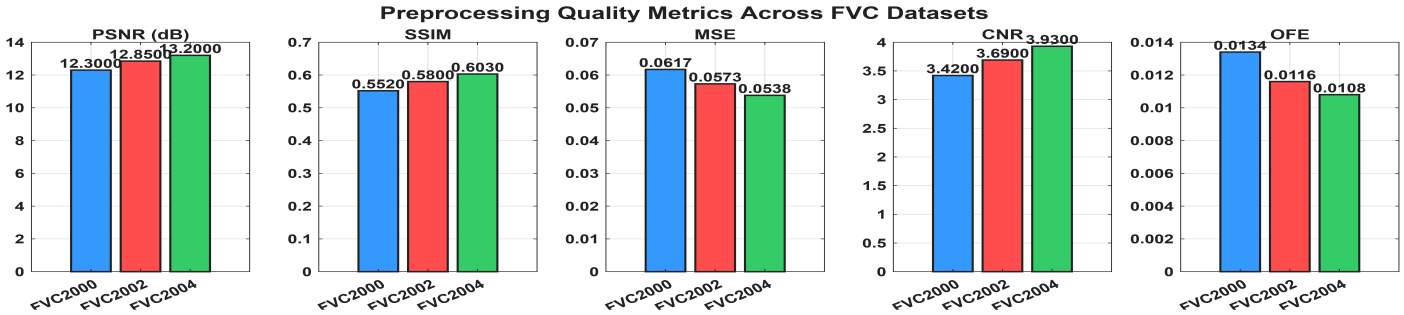

Fig. 6. Graphical representation of preprocessing metrics.

TABLE VI. PREPROCESSING QUALITY METRICS ACROSS FVC DATASETS

Metric	FVC2000	FVC2002	FVC2004
PSNR (dB)	12.30	12.85	13.20
SSIM	0.552	0.580	0.603
MSE	0.0617	0.0573	0.0538
CNR	3.42	3.69	3.93
OFE	0.0134	0.0116	0.0108

Abbreviations: PSNR – Peak Signal-to-Noise Ratio; SSIM – Structural Similarity Index Measure; MSE – Mean Squared Error; CNR – Contrast-to-Noise Ratio; OFE – Orientation Field Error.

TABLE VII. GRAPH-BASED STRUCTURAL METRICS ACROSS FVC DATASETS

Metric	FVC2000	FVC2002	FVC2004
Graph Density	0.0215	0.0268	0.0312
Mean Node Degree	2.34	2.89	3.27
GCN Score (Genuine)	0.742	0.781	0.812
GCN Score (Impostor)	0.284	0.241	0.198
RCF Edge Weight (Mean)	0.712	0.736	0.758
RCF Edge Weight (Std)	0.092	0.085	0.079

TABLE VIII. SENSITIVITY ANALYSIS OF RCF EDGE COMPONENTS

Edge Weight Configuration	EER (%)
Without Correlation Consistency (r_{cc})	2.56
Without Orientation Consistency (o_c)	2.14
Without Frequency Consistency (f_c)	1.83
Full RCF (r_{cc}+o_c+f_c)	1.64

TABLE IX. ABLATION STUDY OF TOPO-GCN FRAMEWORK

Configuration	Precision (%)	Recall (%)	F1 (%)	EER (%)	AUC
Full Model (MSFT + GCN + Hybrid Scoring)	98.68	99.17	98.92	1.64	0.983
Without MSFT Features	96.91	97.42	97.16	2.87	0.964
Without GCN	95.84	96.73	96.28	3.95	0.948
Without Hybrid Scoring	97.12	97.89	97.50	2.41	0.971
Without RCF Graph	94.76	95.88	95.32	4.62	0.932
Without MSFT + GCN	97.45	98.02	97.73	2.18	0.975
Only MSFT	93.28	94.67	93.97	5.84	0.910

B. Evaluation Protocol

Evaluation is carried out under a subject-exclusive protocol, where DB1_B and DB2_B are used for model learning, and DB3_B along with DB4_B are reserved strictly for testing. This partition ensures that no overlap exists between the training and test sets, thus eliminating possible leakages and establishing a realistic scenario for evaluating generalization.

The partitioning method will also provide several differences in the conditions under which samples were obtained within the sub-databases. This permits evaluating a model across distributional differences across FVC Datasets.

The reliability of the performance is derived from the samples in the test by examining the corresponding distributions for genuine and impostor scores. Based on these distributions for the respective test sets, standard performance measures such as AUC (Area Under the Curve) and EER (Equal Error Rate) are calculated to quantify the performance. To assess consistency of these scores across trial instances, confidence intervals are developed using Bootstrap resampling.

Metrics related to minutiae- and verification-level are reported to maintain consistency in the evaluation process.

C. Ablation Study

To assess the performance through ablation analysis, core distinct modules are selectively removed. This experiment confirms that the combination of MSFT-based feature encoding, GCN-based refinement, and hybrid scoring contributes to the effectiveness of the overall system. Therefore, the proposed framework is not a heuristic accumulation but a structurally grounded design.

Additionally, the proposed framework avoids the large-scale labeled data to maintain computational efficiency and generalization capability.

Results of the ablation analysis from Table IX indicate that each core component projects a systematic role in the overall performance of the entire system. The complete model with all cores performs with an F1-score of 98.92%, an EER of 1.64%, and an AUC of 0.983. The removal of the graph structure from the system, decreased the performance with EER = 4.62%, AUC = 0.932, and failed to model the interdependencies between minutiae. These interdependencies are the primary reason for the increase in performance. The removal of the GCN from the system increases the EER to 3.95%, which indicates that the model builds a graph with a larger number of structurally inconsistent candidates. The exclusion of the MSFT features leads to a moderate drop in the quality of the local ridge representation. The addition of the hybrid scoring mechanism further improves the ability to discriminate between candidates, as indicated by an increase in the EER to 2.41% upon its removal. Overall, the results of the analysis show that the sequential degradation of the performance for each configuration confirms that the system has benefited from the complementary effects of feature encoding, graph-based refinement, and adaptive scoring.

V. Conclusion

The proposed Topo-GCN redefines minutiae modeling by explicitly incorporating relational topology through a graph-based fingerprint representation framework. Graph convolutional learning transforms candidate minutiae into a structured graph, effectively capturing the local and global dependencies that are overlooked in conventional point-based representations.

The integration of a compact 14-dimensional feature descriptor with the proposed RCF enables adaptive and physically meaningful edge construction. The hybrid scoring mechanism ensures robust refinement of minutiae under noisy and partial conditions. The adoption of pseudo-labeling further enhances the practicality of the framework by reducing dependence on large annotated datasets. Experimental results across standard FVC benchmarks demonstrate consistent improvements in discriminability and efficiency, validating the effectiveness of topology-driven learning for biometric representation. Unlike deep image-based models that rely on high-dimensional feature extraction, the proposed method achieves competitive performance within a low-dimensional and computationally efficient framework.

Future work will focus on strengthening cross-dataset generalization, incorporating adversarial robustness analysis, and extending the framework toward fully cancelable biometric template generation with formal security guarantees. The findings of this work highlight the importance of structurally-aware representations and establish a foundation for next-generation fingerprint authentication systems.

References

[1] M. Imran, M. S. Umar, and F. Ahmad, "A non-invertible secure template generation using AES encrypted MCC and random triangle projection," *IEEE Access*, vol. 13, pp. 78194–78213, 2025.

[2] S. P. Singh, D. K. Nishad, and S. Khalid, "Enhancing fingerprint identification using fuzzy-ANN minutiae matching," *Measurement: Sensors*, vol. 37, p. 101809, 2025.

[3] C. P. Shahina and B. Mohammed Ismail, "G-Tree indexing and ACO for spatial query," in *Proc. 5th International Conference on Electrical, Electronics, Communication, Computer Technologies and Optimization Techniques (ICEECCOT)*, 2021, pp. 200–203.

[4] M. Imran, M. S. Umar, and S. Malhotra, "Privacy preserving cancellable template generation for crypto-biometric authentication system," *IEEE Access*, vol. 13, pp. 158322–158339, 2025.

[5] S. Bakheet, S. Alsubai, A. Alqahtani, and A. Binbusayyis, "Robust fingerprint minutiae extraction and matching based on improved SIFT features," *Applied Sciences*, vol. 12, no. 12, p. 6122, 2022.

[6] D. Sadhya, "Achieving unlinkability in fingerprint templates via k-anonymity and random projection," *Sadhanā*, vol. 49, no. 3, p. 224, 2024.

[7] Z. Jia and C. Huang, "Automated framework for extracting and restoring minutiae from low-quality fingerprints," *IEEE Signal Processing Letters*, vol. 32, pp. 2194–2198, 2025.

[8] J. J. Engelsma, K. Cao, and A. K. Jain, "Learning a fixed-length fingerprint representation," *IEEE Trans. Pattern Anal. Mach. Intell.*, vol. 43, no. 6, pp. 1981–1997, 2021.

[9] S. A. Grosz and A. K. Jain, "Latent fingerprint recognition: Fusion of local and global embeddings," *IEEE Transactions on Information Forensics and Security*, vol. 18, pp. 5691–5705, 2023.

[10] T. Kim, D. Kwon, A. K. Das, and Y. Park, "Robust and lightweight user authentication scheme using deep learning-based cancelable biometrics in smart home environments," *IEEE Internet Things J.*, 2026.

[11] C. Guo *et al.*, "A novel biometric authentication scheme with privacy protection based on SVM and ZKP," *Computers & Security*, vol. 144, p. 103995, 2024.

[12] M. Ragab *et al.*, "Enhancing cybersecurity in higher education institutions using optimal deep learning-based biometric verification," *Alexandria Eng. J.*, vol. 117, pp. 340–351, 2025.

[13] B. Arslan, "Minutiae-free fingerprint recognition via vision transformers: An explainable approach," *Applied Sciences*, vol. 16, no. 2, p. 1009, 2026.

[14] N. S. Babu, M. Elamparithi, and V. Anuratha, "An intelligent system for fingerprint recognition and verification using dilated convolutional neural network and extreme learning machine," *Int. J. Membrane Sci. Technol.*, vol. 10, no. 2, pp. 2707–2715, 2023.

[15] N. K. Sreeja, "A hierarchical heterogeneous ant colony optimization based fingerprint recognition system," *Intell. Syst. Appl.*, vol. 17, p. 200180, 2023.

[16] R. Garg *et al.*, "Fingerprint recognition using convolution neural network with inversion and augmented techniques," *Syst. Soft Comput.*, vol. 6, p. 200106, 2024.

[17] Y. Qiu, H. Chen, X. Dong, Z. Lin, I. Y. Liao, M. Tistarelli, and Z. Jin, "IFViT: Interpretable fixed-length representation for fingerprint matching via vision transformer," *IEEE Transactions on Information Forensics and Security*, vol. 20, pp. 559–573, 2025.

[18] S. A. Grosz and A. K. Jain, "AFR-Net: Attention-driven fingerprint recognition network," *IEEE Transactions on Biometrics, Behavior, and Identity Science*, vol. 6, no. 1, pp. 30–42, 2024.

[19] RSP, T. Thomas, and S. Emmanuel, "Cancelable biometric template generation using random feature vector transformations," *IEEE Access*, vol. 12, pp. 32064–32079, 2024.

[20] T. Gernot and C. Rosenberger, "Robust biometric scheme against replay attacks using one-time biometric templates," *Computers & Security*, vol. 137, p. 103586, 2024.

[21] T. Sawhney *et al.*, "Fingerprint matching for noisy and distorted patterns using a Siamese network with ResNet50 and multihead attention," *IEEE Access*, vol. 13, pp. 88047–88064, 2025.

[22] S. Salma *et al.*, "Optimizing fingerprint identification: CNNs with raw images versus handcrafted features for real-time systems," *IEEE Access*, vol. 13, pp. 108192–108211, 2025.

[23] A. N. Bonacim *et al.*, "Machine learning for fingerprint ridge counting," *IEEE Trans. Biometrics Behav. Identity Sci.*, vol. 8, no. 1, pp. 60–70, 2026.

[24] X. Guan, J. Feng, and J. Zhou, "Phase-aggregated dual-branch network for efficient fingerprint dense registration," *IEEE Trans. Inf. Forensics Security*, vol. 19, pp. 5712–5724, 2024.

[25] I. Kavati *et al.*, "Design of a fingerprint template protection scheme using elliptical structures," *ICT Express*, vol. 7, no. 4, pp. 497–500, 2021.

[26] A. Wahab *et al.*, "Latent fingerprint enhancement for accurate minutiae detection," *Procedia Comput. Sci.*, vol. 246, pp. 1558–1567, 2024.

[27] S. M. Abdullahi *et al.*, "Cancelable fingerprint template construction using vector permutation and shift-ordering," *IEEE Trans. Dependable Secure Comput.*, vol. 20, no. 5, pp. 3828–3844, 2023.

[28] S. M. Abdullahi, H. Wang, and T. Li, "Fractal coding-based robust and alignment-free fingerprint image hashing," *IEEE Trans. Inf. Forensics Security*, vol. 15, pp. 2587–2601, 2020.

[29] X. Yin *et al.*, "A novel length-flexible lightweight cancelable fingerprint template for privacy-presing authentication systems in resource-constrained IoT applications," *IEEE Internet Things J.*, vol. 10, no. 1, pp. 877–892, 2023.

[30] W. Yang *et al.*, "Biometrics based privacy-preserving authentication and mobile template protection," *Wireless Commun. Mobile Comput.*, vol. 2018, p. 7107295, 2018.

[31] Z. Pan, Y. Duan, X. Guan, J. Feng, and J. Zhou, "Latent fingerprint matching via dense minutia descriptor," in *Proc. IEEE International Joint Conference on Biometrics (IJCB)*, 2024, pp. 1–10.

[32] K. P. Wijewardena, S. A. Grosz, K. Cao, and A. K. Jain, "Fingerprint template invertibility: Minutiae vs. deep templates," *IEEE Transactions on Information Forensics and Security*, vol. 18, pp. 744–757, 2023.

[33] B. Mohammed Ismail, T. Bhaskara Reddy, and B. Eswara Reddy, "Spiral architecture based hybrid fractal image compression," in *Proc. International Conference on Electrical, Electronics, Communication, Computer and Optimization Techniques (ICEECCOT)*, 2016, pp. 21–26.

[34] Z. Ullah, L. Qi, D. Binu, B. R. Rajakumar, and B. M. Ismail, "2-D canonical correlation analysis based image super-resolution scheme for facial emotion recognition," *Multimedia Tools and Applications*, vol. 81, no. 10, pp. 13911–13934, 2022.